Separation Science and Technology
Publication details, including instructions for authors and subscription information:
http://www.informaworld.com/smpp/title~content=t713708471

Effect of Viscosity on Membrane Fluxes in Cross-Flow Ultrafiltration

Shamsuddin Ilias[a]; Keith A. Schimmel[a]; Gervas E. J. M. Assey[a]
[a] Department of Chemical Engineering, North Carolina A&T State University, Greensboro, NC

To cite this Article Ilias, Shamsuddin , Schimmel, Keith A. and Assey, Gervas E. J. M.(1995) 'Effect of Viscosity on Membrane Fluxes in Cross-Flow Ultrafiltration', Separation Science and Technology, 30: 7, 1669 — 1687
To link to this Article: DOI: 10.1080/01496399508010369
URL: http://dx.doi.org/10.1080/01496399508010369

SEPARATION SCIENCE AND TECHNOLOGY, 30(7-9), pp. 1669-1687, 1995

EFFECT OF VISCOSITY ON MEMBRANE FLUXES IN CROSS-FLOW ULTRAFILTRATION

Shamsuddin Ilias , Keith A. Schimmel, and Gervas E.J.M. Assey
Department of Chemical Engineering
North Carolina A&T State University
Greensboro, NC 27407

ABSTRACT

For practical applications of ultrafiltration (UF), an estimation of membrane fluxes under various operational conditions is very important. This study analyzed concentration polarization (CP) as a coupled transport problem with concentration-dependent solute viscosity. Besides the effects of variable viscosity, the model includes the effects of solute osmotic pressure, solute rejection at the membrane surface, and the axial pressure drop. This provides a fundamental understanding of the effects of various operating parameters on concentration polarization and transmembrane flux. A finite-difference solution of the transport equations is presented to model the concentration polarization in a thin-channel UF system. Simulation results for ultrafiltration of Dextran T-70 show that concentration-dependent solute viscosity adversely affects the transmembrane flux and needs to be carefully considered in modeling concentration polarization in membrane filtration.

INTRODUCTION

Ultrafiltration has been an industrial process for over two decades. With the advances in asymmetric membranes and improved engineering designs of UF modules, in many industrial applications UF systems are favored over other conventional separation processes due to their low energy requirement. However,

the flux decline due to 'concentration polarization' and membrane 'fouling' in ultrafiltration processes still remains a major concern in many applications (1). Concentration polarization is the buildup of solutes close to or on the permeable membrane surface due to convective-diffusive transport in the boundary layer. It results in an increase in both resistance to the solvent transport and the local osmotic pressure, which reduces the membrane flux. The operating parameters that usually affect the concentration polarization are velocity, pressure, temperature, and feed concentrations. The optimum operation of UF systems is largely dependent on the management of concentration polarization (2,3). There is a growing need to accurately predict the performance of UF systems for a given operating condition and, if possible, to find ways and means to control the adverse effects of concentration polarization.

The problem of concentration polarization in reverse osmosis and ultrafiltration has been studied theoretically and experimentally by various investigators (4-13). To analyze the problem of concentration polarization, one must understand the transport phenomena at the membrane-solute interface. In modeling cross-flow membrane filtration, usually a thin-channel or tubular membrane module is considered as a model element. In most cases, the model development starts with the decoupling of the momentum equation from the solute continuity equation. The transport equations are usually coupled by the concentration-dependent wall flux condition and solute concentration gradient at the permeable wall. A review of the analytical and numerical works on concentration polarization in cross-flow ultrafiltration and reverse osmosis reveals that the transport equations have been decoupled and simplified by assuming one or more of the following: (a) the wall permeation velocity is assumed constant or piece-wise constant along the axial length; (b) the fluid flow field is approximated by some prescribed functions or by a reduced form of the momentum equation (usually some type of perturbation solution); (c) the wall velocity may depend on osmotic pressure but axial pressure drop is neglected or an approximate pressure drop is used without solving the momentum equation; and (d) the fluid transport properties are assumed constant.

The modeling efforts were essentially based on the decoupling of the transport equations and some major simplifications of wall permeation boundary conditions and did not account for the concentration-dependent viscosity and diffusivity of the solutions in the model development. However, a rigorous concentration polarization model would require solution of coupled transport equations with wall permeation conditions that would depend on transmembrane pressure drop and solute concentration at the membrane interface. Gill, et al., (14) and Bhattacharyya, et al., (15) considered the effect of viscosity and diffusivity in modeling concentration polarization but used simplified flow models that neglected the axial variation of wall permeation velocity and axial pressure drop. Recently, Ilias & Govind (16) studied the concentration polarization in ultrafiltration as a coupled transport problem using constant solute viscosity and diffusivity. In this paper, a new concentration polarization model is presented as a coupled transport problem with concentration-dependent solute viscosity. This analysis will provide a detailed understanding of the role of solute viscosity in the concentration boundary layer and how it relates to transmembrane flux.

MATHEMATICAL FORMULATION

To model the concentration polarization in a thin-channel ultrafiltration (UF) membrane system, it is adequate to use parabolic-type transport equations instead of elliptic equations by using axisymmetric and boundary-layer-type approximations. Thus, for steady flow in a thin-channel UF membrane module, the appropriate governing equations in dimensionless form are given by:

$$\frac{\partial U}{\partial X} + \frac{\partial V}{\partial Y} = 0 \tag{1}$$

$$U\frac{\partial U}{\partial X} + V\frac{\partial U}{\partial Y} = -\frac{dP}{dX} + \frac{1}{Re_{w0}}\frac{\partial}{\partial Y}\left(\bar{\nu}\frac{\partial U}{\partial Y}\right) \tag{2}$$

$$U\frac{\partial C}{\partial X} + V\frac{\partial C}{\partial Y} = \frac{1}{Pe_{w0}}\frac{\partial^2 C}{\partial Y^2} \tag{3}$$

The wall Reynolds number, Re_{w0}, and Peclet number, Pe_{w0}, are based on initial wall permeation velocity, v_{w0}, and half-channel height, h, of the UF membrane module. The last term in the momentum equation, Eq. 2, is the contribution of viscous transport. The concentration-dependent viscosity is included in the viscous transport term. The appropriate boundary conditions for the above system of equations are:

$$U(0,Y) = U_0(Y) = 1.5(1 - Y^2); \quad V(0,Y) = 0; \quad C(0,Y) = 1 \tag{4}$$

$$U(X,1) = 0; \quad V(X,1) = \frac{\Delta P - \Delta \Pi}{R_m}; \quad \left.\frac{\partial C}{\partial X}\right|_{X,1} = \beta Pe_{w0} V_w C_w \tag{5}$$

$$\left.\frac{\partial U}{\partial Y}\right|_{X,0} = 0; \quad \left.\frac{\partial C}{\partial Y}\right|_{X,0} = 0 \tag{6}$$

The boundary conditions, Eq. 4, specify the inlet flow and concentration profiles. The inlet velocity profile may be either uniform (plug flow) or parabolic (Poiseuille flow). The concentration profile of the feed at the inlet is assumed to be uniform. The conditions at the membrane walls for the momentum and solute continuity equations are given by Eq. 5. No slip condition is assumed at the membrane surface. The momentum equation is coupled with the solute continuity equation by the wall flux and solute mass balance of the convective-diffusive transport at the membrane surface with solute rejection coefficient, β. The local wall flux is determined by the axial transmembrane pressure drop, concentration-dependent local osmotic pressure drop across the membrane, and the effective membrane resistance. Symmetry at the centerline for axisymmetric flow and solute transport is reflected in Eq. 6.

METHOD OF SOLUTION

No analytical solution is known for the system of equations, Eqs. 1-3, subject to boundary conditions, Eqs. 4-6. The system of equations is solved by

a finite-difference method implicit in Y. A system of grid lines running in X- and Y-directions (i.e., i and j lines) is imposed on the solution domain. The axial grids are numbered from 1 to m, i.e., i=1 being the inlet boundary (X=0), while i=m is the last axial grid ($X=X_{max}$) of the solution domain. Similarly, transverse grids are numbered from 1 to n, with j=1 being the centerline (Y=0), while j=n is the membrane wall. The discretization schemes of the governing equations and boundary conditions are similar to that described elsewhere (16). For brevity, the finite-difference approximations of Eqs. 1-3 are given here.

$$V_{i,n} = -\sum_{j=2}^{n} \frac{\Delta Y_2}{2\Delta X}(U_{ij} - U_{i-1j} + U_{ij-1} - U_{i-1j-1}) \tag{7}$$

$$A_j U_{ij-1} + B_j U_{ij} + D_j U_{ij+1} = E_j \qquad for \quad 2 \le j \le n-1 \tag{8}$$

$$F_j C_{ij-1} + G_j C_{ij} + H_j C_{ij+1} = I_j \qquad for \quad 2 \le j \le n-1 \tag{9}$$

where the coefficients in Eqs. 8 and 9 are given as:

$$A_j = -a_1 V_{i-1j} + \frac{a_1 a_5(\bar{v}_{i-1j+1} - \bar{v}_{i-1j}) + a_1^2(\bar{v}_{i-1j} - \bar{v}_{i-1j-1})}{Re_{w0}} - \frac{2\bar{v}_{i-1j}}{a_2 Re_{w0}} \tag{10}$$

$$B_j = a_3 V_{i-1j} - \frac{a_3 a_5(\bar{v}_{i-1j+1} - \bar{v}_{i-1j}) + a_1 a_3(\bar{v}_{i-1j} - \bar{v}_{i-1j-1})}{Re_{w0}} + \frac{2\bar{v}_{i-1j}}{a_4 Re_{w0}} + \frac{U_{i-1j}}{\Delta X} \tag{11}$$

$$D_j = a_5 V_{i-1j} + \frac{a_5^2(\bar{v}_{i-1j+1} - \bar{v}_{i-1j}) + a_1 a_5(\bar{v}_{i-1j} - \bar{v}_{i-1j-1})}{Re_{w0}} - \frac{2\bar{v}_{i-1j}}{a_6 Re_{w0}} \tag{12}$$

$$E_j = -\frac{U_{i-1j}^2}{\Delta X} - \frac{1}{2}\frac{dP}{dX}\bigg|_{ij} \tag{13}$$

$$F_j = -a_1 V_{i-1j} - \frac{2}{a_2 Pe_{w0}} \tag{14}$$

$$G_j = a_3 V_{i-1,j} + \frac{2}{a_4 Pe_{w0}} + \frac{U_{i-1,j}}{\Delta X} \tag{15}$$

$$H_j = a_5 V_{i-1,j} - \frac{2}{a_6 Pe_{w0}} \tag{16}$$

$$I_j = U_{i-1,j} \frac{C_{i-1,j}}{\Delta X} \tag{17}$$

with

$$\begin{aligned} a_1 &= \frac{\Delta Y_1}{\Delta Y_2(\Delta Y_1 + \Delta Y_2)}; & a_2 &= \Delta Y_2(\Delta Y_1 + \Delta Y_2) \\ a_3 &= \frac{\Delta Y_1 - \Delta Y_2}{\Delta Y_1 \Delta Y_2}; & a_4 &= \Delta Y_1 \Delta Y_2 \\ a_5 &= \frac{\Delta Y_2}{\Delta Y_1(\Delta Y_1 + \Delta Y_2)}; & a_6 &= \Delta Y_1(\Delta Y_1 + \Delta Y_2) \end{aligned} \tag{18}$$

where

$$\Delta Y_1 = Y_{j+1} - Y_j; \quad \Delta Y_2 = Y_j - Y_{j-1}; \quad \Delta X = X_i - X_{i-1} \tag{19}$$

The derivative boundary conditions at the membrane surface for solute concentration are approximated by a three-point backward-difference formula. At the axis of symmetry, the derivative boundary conditions for fluid flow and solute continuity are given by a three-point forward-difference formula. The finite-difference approximation of the derivative boundary conditions, Eqs. 5 and 6, is given as:

$$U_{i,1} = \frac{U_{i,2}(Y_1 - Y_3)^2 - U_{i,3}(Y_1 - Y_2)^2}{(Y_2 - Y_3)(2Y_1 - Y_2 - Y_3)} \tag{20}$$

$$C_{i,1} = \frac{C_{i,2}(Y_1 - Y_3)^2 - C_{i,3}(Y_1 - Y_2)^2}{(Y_2 - Y_3)(2Y_1 - Y_2 - Y_3)} \tag{21}$$

$$C_{i,n} = \frac{C_{i,n-1}(Y_n - Y_{n-2})^2 - C_{i,n-2}(Y_n - Y_{n-1})^2}{(Y_{n-1} - Y_{n-2})(2Y_n - Y_{n-1} - Y_{n-2} - Pe_{w0}\beta V_{i,n}(Y_n - Y_{n-1})(Y_n - Y_{n-2}))} \quad (22)$$

The grid spacings used in the axial (m-line) and transverse (n-line) directions were established by numerical experimentation. The axial grid spacings were very fine at the channel inlet section and gradually increased along the length of the solution domain. The smallest spacing used was $\Delta X = 1.0 \times 10^{-8}$ and increased along the X-direction by a factor of 1.25. When ΔX reached about 1.0×10^{-3}, uniform spacing was used for the remaining axial section. In the transverse direction near the membrane wall, a grid spacing of $\Delta Y = 1.0 \times 10^{-4}$ was used and the spacings were increased in the transverse direction towards the centerline (half-channel height) by a factor of 1.1. When ΔY reached about 0.04, uniform spacing was used for the remaining transverse length. An iterative procedure was developed to solve the discretized governing equations, Eqs. 7-9, with the necessary boundary conditions. The basic solution procedure is similar to that described elsewhere (16). In the numerical solution, the convergence criteria for the fluid flow and concentration fields were set at $|V_{i,n} - V_w| \leq 10^{-6}$ and $|C_{i,n} - C_w| \leq 10^{-6}$, respectively. No numerical instabilities were encountered in any of the simulation runs.

RESULTS AND DISCUSSION

The important variables that affect the performance of membrane filtration are feed flow rates, feed concentration, operating pressure, solute viscosity and diffusivity, and osmotic pressure. In this work, the effect of solute concentration on diffusivity is neglected. It has been argued that the variation of solute diffusivity with concentration is much smaller than that of viscosity (14). Thus, the assumption of constant solute diffusivity does not seem to affect the qualitative results of the effect of variable viscosity in membrane filtration. In this paper, we have made an attempt to describe the concentration polarization in thin-channel

ultrafiltration as a coupled convective-diffusive transport problem and presented a finite-difference solution of the model equations.

Table 1 provides a summary of membrane module dimensions and input data used in this study. The viscosity and osmotic pressure functions used for Dextran T-70 are those reported in the works of Clifton, et al., (17) and Ogston & Preston (18), respectively. The inlet velocity profile was assumed to be parabolic. To compare the effects of variable viscosity and constant viscosity on cross-flow ultrafiltration, parametric studies were performed for a wide range of operating conditions.

Figure 1 is a plot of dimensionless wall permeation velocity, $V_w = v/v_{w0}$, against distance downstream, x, with feed solute concentration as a parameter. The feed solute concentrations ranged from 0.1 wt % to 5.0 wt %. With a feed velocity of 1 m/s, the variation of wall permeation velocity with axial distance is shown for three initial wall permeation velocities, 10^{-6} m/s, 10^{-5} m/s, and 10^{-4} m/s, for the case of constant viscosity. In Figure 2, the same plots are given for the case of variable viscosity. A wide range of initial wall permeation velocities is used to include the lower and upper limits of ultrafiltration conditions. A wall permeation velocity of 10^{-6} m/s definitely represents reverse osmosis conditions, while a permeation velocity of 10^{-4} m/s is probably under microfiltration conditions.

For both constant and variable solute viscosity models, the wall permeation velocity, and hence, the transmembrane flux decreases along the axial direction for all feed concentrations and initial wall permeation velocities. The general trend is that, for a given initial wall permeation velocity, the transmembrane flux decreases rapidly with increasing feed concentrations. In the case of high-permeability membranes (e.g. $v_{w0} = 10^{-4}$ m/s), the decline in transmembrane flux may take place within a short distance downstream. In the case of low permeability membranes (e.g., $v_{w0} = 10^{-6}$ m/s), the transmembrane flux may remain unaffected at the entrance, but the flux decreases further downstream. Comparing Figure 1 with Figure 2, it is apparent that the onset of flux decline

TABLE 1. DIMENSION OF MEMBRANE MODULE AND INPUT DATA

System:
Thin-Channel UF Module
Channel Half-height (h): 0.001 m
Membrane Solute Rejection Coefficient, $\beta = 1.0$
Operating Pressure: 5.0×10^5 Pa
Feed: Dextran T-70 Aqueous Solution
Concentration Range: 0.1 wt % - 5.0 wt %
Feed Velocity (u_0): 1 m/s
Initial Wall Permeation Velocity (v_{w0}): 10^{-6} m/s - 10^{-4} m/s

Viscosity Model (17):
$\mu = 0.0009086\,[1 + 0.01c \exp(0.08678c + 3.313)]$
where μ is in Pa·s and c is in wt %

Osmotic Pressure Model (18):
$\pi \times 10^{-5} = 0.6353c + 12.636c^2 + 49.55c^3$
where π is in Pa

along the membrane length takes place earlier in the case of variable viscosity. For example, with $v_{w0} = 10^{-5}$ m/s, and $c_0 = 1.0$ wt %, the initial transmembrane flux drops down to 50% at 98 cm distance downstream for the constant viscosity case, while for the variable viscosity case, this reduction in transmembrane flux takes place within 27 cm of the entrance. This clearly demonstrates how the concentration-dependent solute viscosity adversely affects the transmembrane flux in filtration.

The variation of dimensionless wall solute concentration, $C_w = c_w/c_0$, along the distance downstream is shown in Figures 3 and 4 for the constant- and variable-viscosity models, respectively. The conditions are the same as used in Figure 1. The significant difference between the constant and variable viscosity models is again obvious. For a given initial wall permeation velocity, the wall solute concentration increases along the axial length for all feed concentrations.

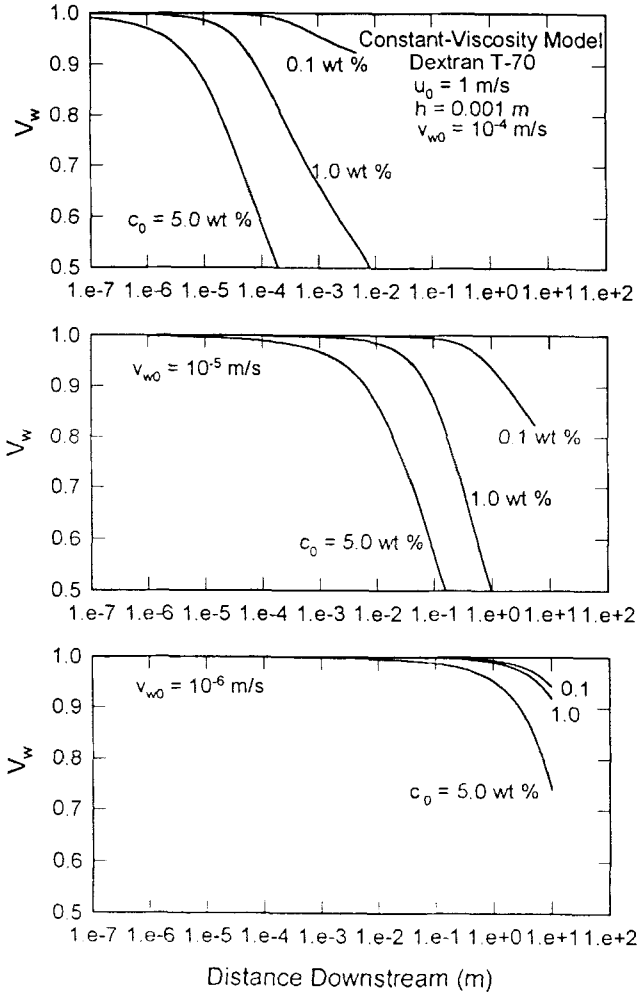

FIGURE 1. Variation of dimensionless transmembrane flux (wall permeation velocity) along the axial length of a thin-channel UF module at three feed concentrations (constant-viscosity model).

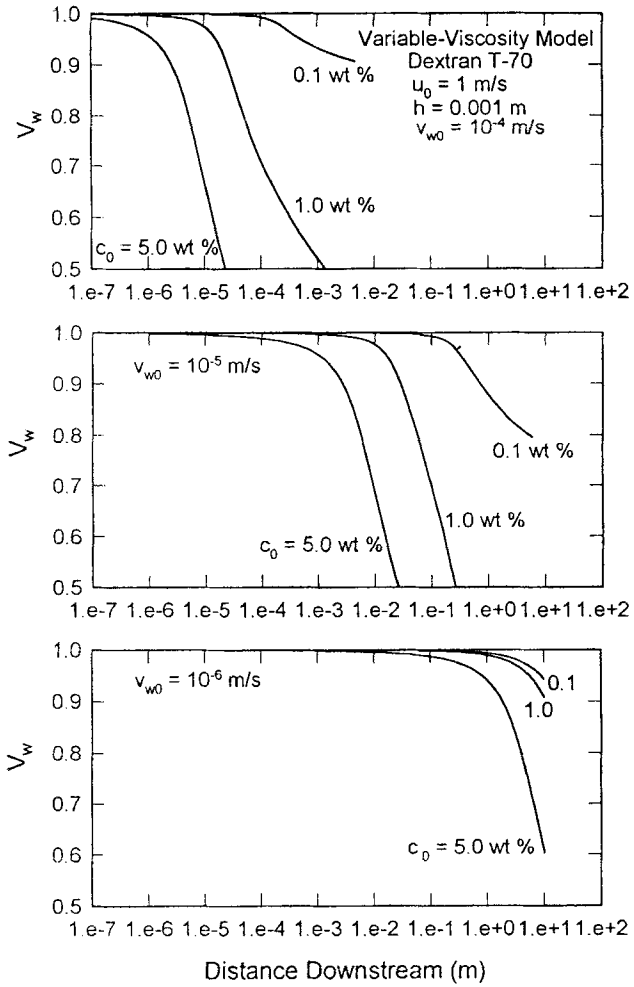

FIGURE 2. Variation of dimensionless transmembrane flux (wall permeation velocity) along the axial length of a thin-channel UF module at three feed concentrations (variable-viscosity model).

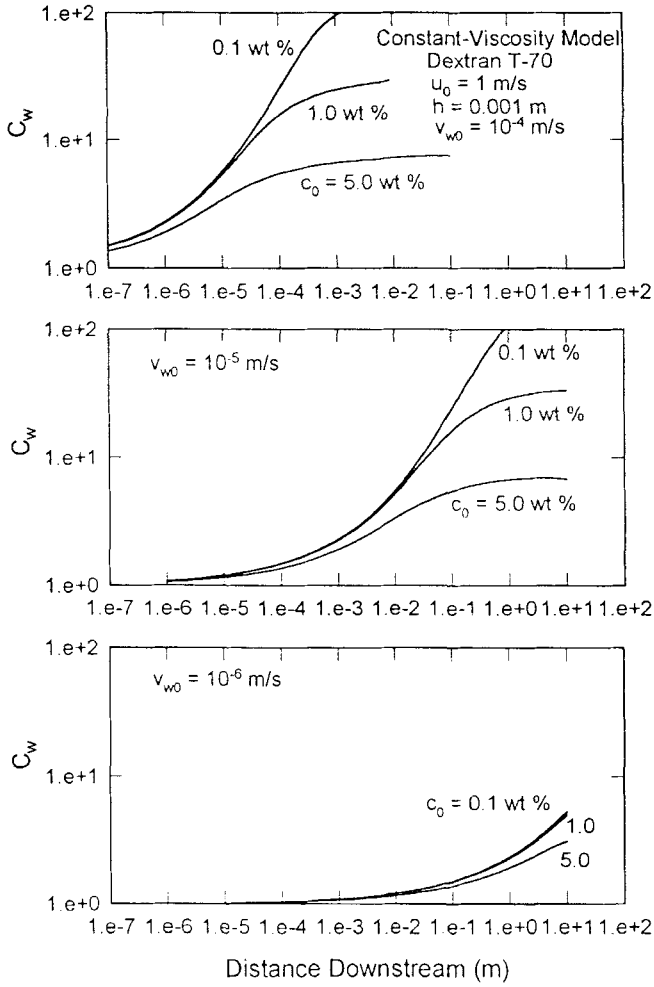

FIGURE 3. Variation of dimensionless solute concentration at the membrane wall along the axial length of a thin-channel UF module at three feed concentrations (constant-viscosity model).

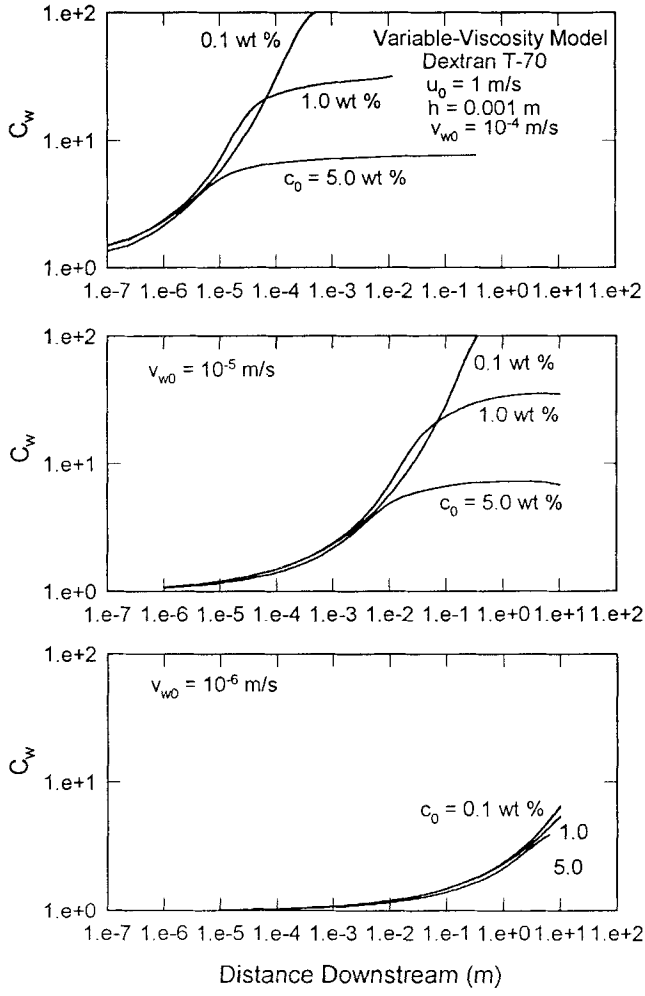

FIGURE 4. Variation of dimensionless solute concentration at the membrane wall along the axial length of a thin-channel UF module at three feed concentrations (variable-viscosity model).

At the low initial wall permeation velocity (e.g., $v_{w0} = 10^{-6}$ m/s), there is no appreciable difference between the two models and the wall solute concentration is only two to three times that of the feed solution. For the constant-viscosity model (Figure 3), for example, at x = 50 cm from the entrance, the wall concentrations (c_w) are 8.5, 1.9, and 0.2 wt % for feed concentrations of 5, 1, and 0.1 wt %, respectively. For the variable-viscosity model (Figure 4) at x = 50 cm, these concentrations are 9.1, 2.0, and 0.2 wt % for feed concentrations of 5, 1, and 0.1 wt%, respectively. However, the buildup of wall solute concentrations is more dramatic in the case of high initial wall permeation velocities. At high wall permeation velocities, the concentrations build up rapidly with the loss of permeate. For example, at a wall permeation velocity of 10^{-5} m/s, and at x = 50 cm, the constant-viscosity model predicts wall solute concentrations of 32.6, 26.2, and 7.6 wt % for inlet feed concentrations of 5, 1, and 0.1 wt %, respectively. For the same conditions, the variable-viscosity model (Figure 4) predicts wall solute concentrations of 35.8, 31.9, and 12.3 wt %, for feed concentrations of 5, 1, and 0.1 wt %, respectively.

The decline of transmembrane flux and increase in wall solute concentration along the axial direction largely depend on the magnitude of initial wall permeation velocity. At low initial wall permeation velocity (as in reverse osmosis, $v_{w0} < 10^{-6}$ m/s), the difference between the variable- and constant-viscosity models is not significant. Therefore, the assumption of constant viscosity in reverse osmosis should be satisfactory (5). However, when the wall permeation velocities are more typical of ultrafiltration, with loss of permeate, the solute viscosity becomes a concentration-dependent variable that greatly affects the buildup of wall solute concentration and transmembrane flux. Under this condition, a constant-viscosity model will grossly overestimate the transmembrane flux and, also, underestimate the concentration buildup in a typical ultrafiltration operation. The concentration polarization is defined as (6):

$$C_P = \frac{c_w}{c_0/(1-X)} = 1 = C_w(1 - X) = 1 \qquad (23)$$

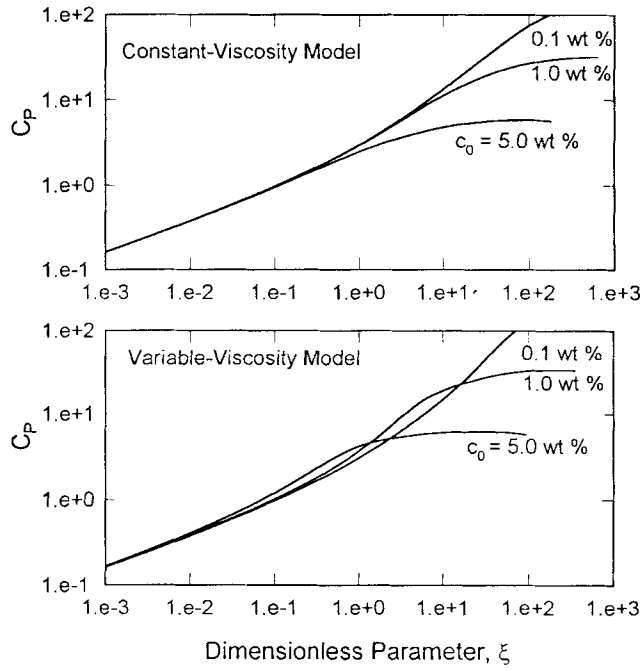

FIGURE 5. Effect of feed concentration on concentration polarization plotted as a function of dimensionless parameter, ξ for the cases of constant- and variable-viscosity models for Dextran T-70.

where the term, $c_0/(1\text{-}X)$ is the mixing-cup average solute concentration. To be consistent with other published works (5,14,19), the dimensionless axial distance (X) or the fraction of water removed at a given value of x is rescaled as:

$$\xi = 3\frac{x}{h}\left(\frac{v_{w0}}{u_0}\right)\left(\frac{v_{w0}h}{D_0}\right)^2 \tag{24}$$

The function ξ is a dimensionless quantity which includes the effect of the variable channel height (h), feed velocity (u_0), solute diffusivity (D_0), and initial wall permeation velocity (v_{w0}). Thus, a plot in terms of ξ is essentially a multiparameter representation of a large number of other graphs that could be

drawn to illustrate the effect of a single parameter on the concentration polarization.

Figure 5 presents the results of concentration polarization, C_p, as a function of dimensionless parameter, ξ, for both the constant- and variable-viscosity models. For any value of c_0, C_P increases with the fraction of water removed (or dimensionless longitudinal position) and then levels out at an asymptotic value of C_P. The asymptote corresponds to the distance far downstream. This distance is approached at relatively low values of water removal when c_0 is large. On the other hand, at low values of c_0, the asymptotic polarization is approached only as water removal approaches unity. A close review of Figure 5 indicates that there is a significant difference between the values of C_P obtained assuming the constant viscosity and variable viscosity, particularly at higher inlet feed concentrations.

CONCLUSIONS

In cross-flow ultrafiltration, concentration-dependent solute viscosity may play an important role in evaluating the performance of such systems. The present study analyzed concentration polarization as a coupled transport problem with concentration-dependent solute viscosity. This provides fundamental information for the analysis of ultrafiltration systems. The simulation results indicate that there is a significant difference between the values of wall permeation velocity (v_w) and solute wall concentration (c_w) obtained by the constant-viscosity and variable-viscosity models. The present model can be readily extended to hollow-fiber and tubular ultrafiltration systems. In any ultrafiltration operation, if the solution shows a strong dependence of viscosity on concentration, a constant-viscosity assumption may grossly over estimate the transmembrane flux and underestimate the effect of concentration polarization.

NOTATIONS

A_j coefficient of $U_{i,j-1}$ of Eq. 8 as defined by Eq. 10
a_i constants in Eqs. (10-12) and (14-16) as defined by Eq. 18, for $i=1,6$

B_j coefficient of $U_{i,j}$ of Eq. 8 as defined by Eq. 11
C dimensionless solute concentration, c/c_0
C_w dimensionless wall solute concentration, c_w/c_0
C_P concentration polarization as defined by Eq. 23
c solute concentration, wt %
c_w surface solute or gel concentration, wt %
c_0 feed concentration at inlet, wt %
D_0 solute diffusivity, $cm^2 \cdot s^{-1}$
D_j coefficient of $U_{i,j+1}$ of Eq. 8 as defined by Eq. 12
E_j a constant in Eq. 8 as defined by Eq. 13
F_j coefficient of $C_{i,j-1}$ of Eq. 9 as defined by Eq. 14
G_j coefficient of $C_{i,j}$ of Eq. 9 as defined by Eq. 15
H_j coefficient of $C_{i,j+1}$ of Eq. 9 as defined by Eq. 16
I_j a constant in Eq. 9 as defined by Eq. 17
p pressure, Pa
p_o pressure on the permeate side, Pa
Δp transmembrane pressure, $(p-p_o)$, Pa
ΔP dimensionless transmembrane pressure, $2(p-p_o)/\rho u^2_0$
Pe_{w0} Peclet number based on initial wall permeation velocity, $v_{w0}h/D_0$
r_m effective membrane resistance, $Pa/cm \cdot s^{-1}$
R_m normalized effective membrane resistance, $2v_{w0}r_m/\rho u^2_0$
Re_{w0} wall Reynolds number based initial wall permeation velocity, $v_{w0}h/\nu_0$
u axial velocity component in x-direction, $cm \cdot s^{-1}$
u_0 average inlet velocity at $x=0$, $cm \cdot s^{-1}$
U dimensionless axial velocity, u/u_0
v velocity in y-direction, $cm \cdot s^{-1}$
v_{w0} initial wall permeation velocity, $cm \cdot s^{-1}$
V dimensionless transverse velocity, v/v_{w0}
x axial direction
X dimensionless axial direction (or fraction of water removed at x), $v_{w0}x/u_0h$
ΔX finite-difference grid spacing in X-direction as defined by Eq. 19
y transverse direction
Y dimensionless transverse direction, y/h
ΔY_1 finite-difference grid spacing in Y-direction as defined by Eq. 19
ΔY_2 finite-difference grid spacing in Y-direction as defined by Eq. 19
β solute rejection coefficient at the membrane surface
ν kinematic viscosity of solution (μ/ρ), $cm^2 \cdot s^{-1}$
ν_0 reference kinematic viscosity of feed at channel inlet (μ_0/ρ), $cm^2 \cdot s^{-1}$
$\bar{\nu}$ dimensionless kinematic viscosity (ν/ν_0)
μ dynamic viscosity of solution, $g \cdot cm^{-1} \cdot s^{-1}$
μ_0 reference dynamic viscosity of feed at channel inlet, $g \cdot cm^{-1} \cdot s^{-1}$
π osmotic pressure of the solute in solution, Pa
π_o osmotic pressure of permeate, Pa
$\Delta\Pi$ transmembrane osmotic pressure, $2(\pi-\pi_o)/\rho u^2_0$
ρ density of feed solution, $kg \cdot m^{-3}$
ξ dimensionless parameter as defined by Eq. 24

REFERENCES

1. C.A. Smolders and Th. van den Boomgaard, J. Memb. Sci. **40**, 121 (1989).

2. H. Reihanian, C.R. Robertson and A.S. Michaels, J. Memb. Sci. **16**, 237 (1983).

3. A. Suki, A.G. Fane and C.J.D. Fell, J. Memb. Sci. **21**, 269 (1984).

4. U. Merten, Ind. Eng. Chem. Fundam. **2**, 229 (1963).

5. T.K. Sherwood, P.L.T. Brian, R.E. Fisher and L. Dresner, Ind. Eng. Chem. Fundam. **4**, 113 (1965).

6. P.L.T. Brian, Ind. Eng. Chem. Fundam. **4**, 439 (1965).

7. W.N. Gill, C. Tien and D.W. Zeh., Ind. Eng. Chem. Fundam. **4**, 433 (1965).

8. W.N. Gill, L.J. Derzansky and M.R. Doshi, "Convective Diffusion in Laminar and Turbulent Hyperfiltration (Reverse Osmosis) Systems," In Surface and Colloid Science, E. Matijevic (ed.), Wiley, New York, **4**, 261, (1971).

9. M.R. Doshi and W.N. Gill, Chem. Eng. Sci. **30**, 467 (1975).

10. W-F. Leung and R.F. Probstein, Ind. Eng. Chem. Fundam. **18**, 274 (1979).

11. C. Kleinstreuer and M.S. Paller, AIChE J. **29**, 529 (1983).

12. A.G. Fane, J. Memb. Sci. **20**, 249 (1984).

13. R.P. Ma, C.H. Gooding and W.K. Alexander, AIChE J. **31**, 1728 (1985).

14. W.N. Gill, D.E. Wiley, C.J.D. Fell and A.G. Fane, AIChE J. **34**, 1563 (1988).

15. D. Bhattacharyya, S.L. Back, R.I. Kemode and M.C. Roco, J. Memb. Sci. **48**, 231 (1990).

16. S. Ilias and R. Govind, Sep. Sci. Tech. **28**, 361 (1993).

17. M.J. Clifton, N. Abidine, P. Aptel and V. Sanchez, J. Memb. Sci. **21**, 233 (1984).

18. A.G. Ogston and B.N. Preston, Biochem. J. **183**, 1 (1979).

19. R. Singh and R.L. Laurence, Int. J. Heat Mass Transfer **22**, 721 (1979).